JOURNAL OF GEOPHYSICAL RESEARCH, VOL. 95, NO. B4, PAGES 4647–4656, APRIL 10, 1990

Slant Stack Velocity Analysis of Shot Point 16 From the 1986 PASSCAL Ouachita Experiment

J. A. LYSLO[1] AND R. L. NOWACK

Department of Earth and Atmospheric Sciences, Purdue University, West Lafayette, Indiana

A τ-P slant stack algorithm is applied to shot point 16 of the 1986 PASSCAL Ouachita experiment to determine the optimal one-dimensional velocity structure. Several enhancements to a standard slant stack algorithm are used to image a one-dimensional velocity function from the shot point gathered data. Because only postcritical reflections and refractions are needed to image a velocity function, significant muting of precritical energy is performed, which reduces the effect of noise in calculating the stack. For data sets with long offsets, scaling the data by a factor equal to or greater than offset distance compensates for the effects of geometrical spreading and attenuation. This enhances imaging of the deeper regions of the velocity model and balances amplitudes across the shot point gather. Finally, ray parameter-depth images can have difficulty imaging higher velocities, since for higher velocities, a small change in ray parameter results in a large increment in velocity. This problem is overcome by slant stacking in equal increments of velocity instead of ray parameter. The enhanced slant stack algorithm is applied to shot point 16 of the 1986 PASSCAL Ouachita data set, which sufficiently satisfies the assumption of lateral homogeneity based on previous studies of the region. Other velocity models are found to be consistent with the envelope of velocity function imaged by the slant stack method. Maximum amplitudes on the τ-P image are used as a constraint to delineate a more detailed velocity model. A seven-layer velocity model is derived for shot point 16 which is found to be similar to those of others who have studied the area. The top three layers are sediments associated with the gulf coastal plain, followed by a thick layer derived from sedimentation associated with the closing of the proto-Gulf of Mexico and the associated Ouachita orogeny. The determination of a more detailed velocity function from the envelope suggests somewhat higher velocities in the lower crustal layer than previous studies. However, given the one-dimensional assumptions of the method, as well as the signal to noise ratio of the data, the velocity envelope is the most important constraint on the velocity models and tectonic interpretation provided by this analysis.

INTRODUCTION

The τ-P method is a robust procedure for determining one-dimensional velocities from common midpoint or common shot point seismic data. Some of the papers which describe the slant stack method include *Phinney et al.* [1981], *Diebold and Stoffa* [1981], *Stoffa et al.* [1981], *Clayton and McMechan* [1981], and *McMechan et al.* [1982]. The slant stack method of *Clayton and McMechan* [1981], which will be used in this study, linearly transforms the time-offset (T-X) wave field into the τ-P domain, where τ is intercept time and P is ray parameter. In order to obtain the velocity structure from the data, the τ-P wave field is downward continued with a nonlinear stretch into the Z-P domain, where Z is depth. The velocity function is imaged in the Z-P wave field as the curve of maximum energy, or τ curve. Several enhancements to the slant stack method of *Clayton and McMechan* [1981] are used in this paper to better image a velocity versus depth function, including muting, amplitude scaling, and slant stacking in equal increments of velocity instead of ray parameter.

This enhanced slant stack algorithm is used to image the velocity structure from shot point gather 16 of the Program for Array Seismic Studies of the Continental Lithosphere (PASSCAL) Ouachita lithospheric seismic study. This experiment was conducted in May 1986 to gain a better understanding of the geologic and tectonic evolution of the southern continental margin of the United States. The experiment extends from southwestern Arkansas, in the Southern Ouachita Mountains, for 200 km into northern Louisiana, on the gulf coastal plain. A location map of the study is given by *Lutter et al.* [this issue] and *Lutter and Nowack* [this issue]. The data set consists of seismograms from two 100-km-long recording deployments, with each deployment having 400 seismic group recorders (SGR) at an average spacing of 0.25 km. A total of 29 shots were fired into the recording arrays with near-vertical reflections, wide-angle reflections, and refractions all being recorded. A more detailed description of the experiment is given by *Braile et al.* [1987], as well as *Lutter et al.* [this issue] and *Lutter and Nowack* [this issue].

The geotectonic history of the study area is long and complex. It involves Eocambrian rifting and the development of a passive margin during the early Paleozoic, followed subduction and plate collision during the late Paleozoic. A second rifting event started in the Triassic, followed by passive margin development which has continued through the present [see *Keller et al.*, 1989]. This study, along with those of *Lutter et al.* [this issue] and *Lutter and Nowack* [this issue] are designed to image seismically the crustal structure and provide constraints on possible tectonic interpretations.

Other studies of this data set, including the studies of *Lutter et al.* [this issue] and *Lutter and Nowack* [this issue], as well as by *Jardine* [1988] and *Plappert* [1987], have generally made assumptions concerning the number of layers in their models or velocity distribution within layers. Using the slant stack velocity analysis, the primary assumption about the velocity structure is that the region to be imaged is laterally homogeneous. After development of an enhanced slant stack algorithm, it will be shown that the data of shot point 16 sufficiently satisfy this assumption. Because there are no assumptions about the number

[1]Now at Exxon Company, U.S.A., Denver, Colorado.

Paper number 89JB03781.
0148-0227/90/89JB-03781$05.00

of layers or the vertical velocity distribution within layers, the slant stack method has the potential to produce a more detailed velocity function. In addition, the slant stack algorithm used does not require the picking of travel times. However, as with other methods, there will still be sensitivity to the signal to noise ratio in the data. The detailed velocity functions presented in this paper have been interpreted from an envelope of velocity functions imaged by the slant stack method. The velocity function and its envelope provide constraints on the geologic interpretation.

DEVELOPMENT OF THE SLANT STACK ALGORITHM

The first step of imaging a velocity versus depth function is the calculation of the slant stack. A slant stacking algorithm starts with a time versus offset (*T-X*) data set, either in common midpoint, common shot point, or common receiver format. By a linear process related to the radon transform, the data are transformed into a τ-P wave field, where $P = dt/dx$ is the ray parameter and t is the intercept time [*Chapman*, 1981]. In a *T-X* wave field, every ray parameter represents a different slope through the wave field. Thus each *P* trace in the τ-P wave field represents the stack of *T-X* data along a unique slope for a series of intercept times.

Slant stacks are usually performed using equal increments of ray parameter, which yields a plot of τ versus *P*. The τ versus velocity function can be obtained from this plot since the ray parameter is the reciprocal of horizontal velocity. However, there can be a problem when analyzing data for higher velocities. As the ray parameter becomes smaller (higher velocities), each equal step in ray parameter is a larger step in velocity. This results in a lack of sampling of the faster portions of the velocity function when using equal increments of ray parameter. For example, between $P = 0.15$ s/km and $P = 0.05$ s/km, the change in velocity is 13.3 km/s, whereas between $P = 0.35$ s/km and $P = 0.25$ s/km, the change in velocity is only 1.14 km/s. *Plappert* [1987] and *Jardine* [1988], as well as *Lutter and Nowack* [this issue], have shown that the majority of the Ouachita crustal section has velocities in excess of 5.0 km/s (P 0.20 s/km). Therefore, in order to sample adequately these velocities, slant stacks in this study are done in equal increments of velocity. The increased sampling of the faster parts of the velocity function by constant velocity increments allows for a more detailed interpretation of the final velocity-depth function.

The limit on the smallest justifiable increment of velocity is determined by the smallest increment of ray parameter and the fastest expected velocity in the data. The smallest increment of ray parameter, ΔP, is determined from [see *Phinney and Jurdy*, 1979; *Brocher et al.*, 1982]

$$\Delta P = (fX)^{-1} \tag{1}$$

where f is the dominant frequency and X is the record length.

For the analysis of shot point gather 16 in this study, $f = 10$ Hz and $X = 135$ km, thus $\Delta P = 0.00074$ s/km. The fastest velocity that is expected in the data set is approximately 8.2 km/s, and at this velocity the minimum resolvable ΔV is 0.05 km/s. Because at all slower velocities the minimum resolvable ΔV will be smaller, a value of 0.05 km/s is used in this study.

The second part in imaging a velocity function is the downward continuation of the τ-P wave field into a *Z-P* wave field, where Z is depth. *Clayton and McMechan* [1981] implement the downward continuation with a user-supplied velocity versus depth function that is used to calculate a nonlinear stretch for each ray parameter trace. After each downward continuation, the velocity versus depth function is updated to match the locus of points of maximum amplitude on the downward continued τ-P wave field. This locus of points is also known as the tau curve [see *Bessonova et al.*, 1976]. Convergence is reached, and the velocity function is imaged, when the input velocity function is the same as locus of maximum amplitude on the output *Z-P* wave field. Since each iteration in the process uses the original slant stacked wave field for downward continuation, convergence is not so dependent on choice of the initial velocity model.

There are several assumptions and problems with the method of *Clayton and McMechan* [1981]. When calculating the velocity function from the downward continued wavefield, the imaged medium is assumed to be laterally homogeneous. Deviations from this assumption will introduce error. The *Clayton and McMechan* [1981] algorithm also introduces some error by assuming a constant phase shift for postcritical reflections. *Brocher et al.* [1982] have shown that the *Clayton and McMechan* [1981] algorithm is only strictly valid for a smoothly varying media. True layers without gradients are not properly imaged due to the phase shift assumptions. However, *McMechan et al.* [1982] have illustrated that even when these assumptions are not exactly met, the method is robust enough that a meaningful velocity versus depth curve can still be imaged.

The formula to calculate the downward continuation, as given by *Clayton and McMechan* [1981], is

$$S(P, z) = \int_{-\infty}^{\infty} S(P,\omega) e^{-i\omega\psi(P,z)} \frac{d\omega}{2\pi} \tag{2}$$

where

$$\psi(P, z) = 2 \int_0^z \left[v^{-2}(z) - P^2\right]^{\frac{1}{2}} dz \tag{3}$$

P	ray parameter;
$v(z)$	velocity versus depth function given manually for downward continuation;
$S(P,w)$	Fourier transform of a slant stack trace $S(P,t)$;
w	angular frequency;
$S(P,z)$	ray parameter - depth wave field.

The downward continuation is only applied for P less than or equal to $v(z)$.

The continuation in (2) is posed as an integration in the frequency domain, which can be very computationally intensive. *Clayton and McMechan* [1981] note that (2) can be solved in the time domain as a moveout correction applied to the slant stacked data but do not elaborate on this implementation. Equation (2) can be converted to the time domain using Parseval's theorem. Parseval's theorem can be written as [see *Bracewell*, 1978]

$$\int F(\omega)\, G^* \frac{d\omega}{2\pi} = \int f(t)\, g^*(t)\, dt \tag{4}$$

Given (2) and using (4), then

$$S(P, z) = \int S(P,\tau)\, \delta(\tau - \psi(P, z))\, d\tau \tag{5}$$

Therefore

$$S(P, z) = S[P, \tau = \psi(P, z)] \quad (6)$$

In the time domain, the $\psi(P,z)$ function is a moveout correction, and it acts as a direct map from τ, the intercept time, to depth. The time domain method is more straightforward and requires less computing time than the frequency domain approach. In this study, the *Clayton and McMechan* [1981] process is used except that the wave field that is downward continued is a τ-V wave field instead of a τ-P wave field, which results in an Z-V wave field instead of a Z-P wave field.

APPLICATION OF SLANT STACK TO THE PASSCAL DATA SET

A primary assumption of *Clayton and McMechan*'s [1981] downward continuation process yielding the correct velocity-depth function is lateral homogeneity. A question which must be addressed is whether the shot point 16 Ouachita data satisfy this condition sufficiently to result in an accurate one-dimensional velocity model. There is evidence from other studies on the PASSCAL data set as well as other studies in the region which indicate that the crustal structure imaged by shot point 16 is approximately one-dimensional.

Several studies of the PASSCAL data have indicated that the crust imaged beneath shot point gather 16 is approximately one-dimensional. *Jardine* [1988] picked travel times on every shot point gather of the data set and forward modeled the arrival times using ray tracing. The resultant model and ray trace for shot point 16 are shown in Figure 1. This model is approximately one-dimensional over the portion of the crust imaged by shot point 16. *Plappert* [1987] imaged a basically horizontally stratified crust in the vicinity of shot point 16 using a CDP stack of the entire PASSCAL data set.

The lateral homogeneity of the crust in the vicinity of shot point 16 is also supported by gravity data. *Jardine* [1988] found that a density model having a very similar configuration to his velocity model could be used to match the Bouguer gravity

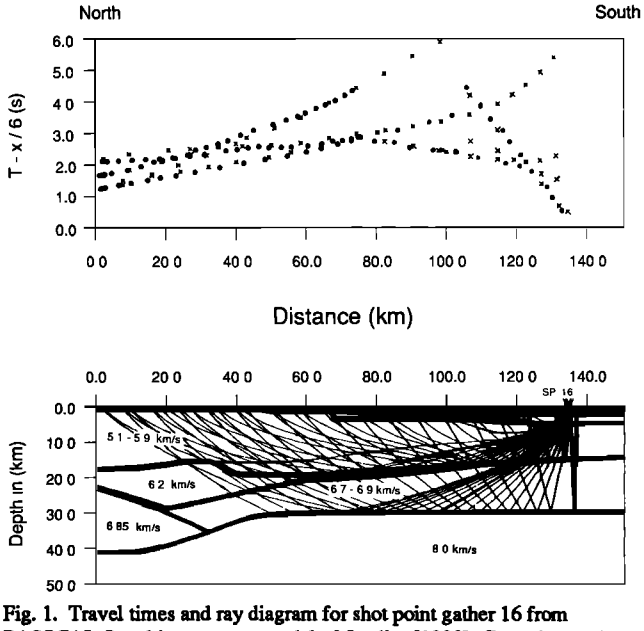

Fig. 1. Travel times and ray diagram for shot point gather 16 from PASSCAL Ouachita ray trace model of *Jardine* [1988]. Dot, observed; Cross, theoretical.

along the PASSCAL profile. *Kruger and Keller* [1986] modeled Bouguer gravity in a profile parallel to the PASSCAL data set but slightly to the west and also found that the crust lacked significant lateral heterogeneities in this region. Given these forward modeling results, the region beneath shot point gather 16 should sufficiently satisfy the lateral homogeneity assumption well enough for the slant stack wave field analysis to yield a valid one-dimensional velocity structure.

Although these other studies have all depicted similar models, this study is important because it is a nonbiased method of extracting crustal velocity structure. The previous studies of the data are all based at some point on the picking of arrival times. The slant stack method requires no picking of arrivals and should image more details of crustal velocity structure. It also provides valuable control on results obtained by travel time methods. However, as with other methods, there will be sensitivity to signal to noise ratio of the data.

The combined northern and southern deployments of shot point 16 (see Figure 2) provide continuous data coverage from the northern end of the PASSCAL profile to the shot point, located 135 km to the south. In Figure 2, every other trace is plotted for clarity and excessively noisy traces also have not been plotted. The initial slant stack of the data in equal ray parameter increments is shown in Figure 3 and lacks a well-defined τ curve, suggesting the need for the application of other enhancements.

The postcritical reflections and refractions are the important arrivals in imaging the velocity-depth function. A large part of the wave field does not contain these arrivals, thus only contributing noise to the slant stacked wave field. With this in mind, large-scale mutes, outlined on Figure 2, were applied to the data. The top of the mute was chosen to guarantee that all of the first arrivals were included in the slant stack, and the bottom was selected to include most postcritical reflections and some precritical reflections.

In addition to muting, another enhancement is to scale the input T-X seismograms by distance which counteracts the effects of geometrical spreading. A greater scaling would compensate for any attenuation as well. The lower sections of any deep velocity model are imaged by the far offset traces, where deep reflectors are postcritical. Scaling by a factor equal to or greater than offset distance enhances the amplitudes of these far-offset traces and increases the amplitudes of the deeper parts of the τ curve. A value of $X^{1.3}$ (where X is offset distance) was selected for this study in order to equalize qualitatively the average amplitudes across the shot point gather. No attempt was made to tie this value into an average apparent attenuation value for the crust as this subject is beyond the scope of this study.

A third modification was made by stacking in equal increments of velocity instead of ray parameter, which enhances the imaging of the higher velocity parts of the model. The velocity increment selected for this study is 0.05 km/s, based on the analysis developed earlier. The resultant wave field, with these enhancements is an improvement over the initial wave field since the curve of maximum energy, or the τ curve, is more clearly defined (see Figure 4).

Some interpretations of the slant stack can be made even before downward continuing the τ-V wave field to depth. In the slant stack, straight lines in T-X, such as refractions, collapse into points in the τ-V domain. Each interface should have a locus of energy on the τ curve associated with a collapsed refraction and several of these loci are found on Figure 4. The first one, although slightly diffuse, is at approximately 5.9-6.0 km/s and a τ of 3.0 s, followed by a locus at approximately 6.8 km/s and τ of

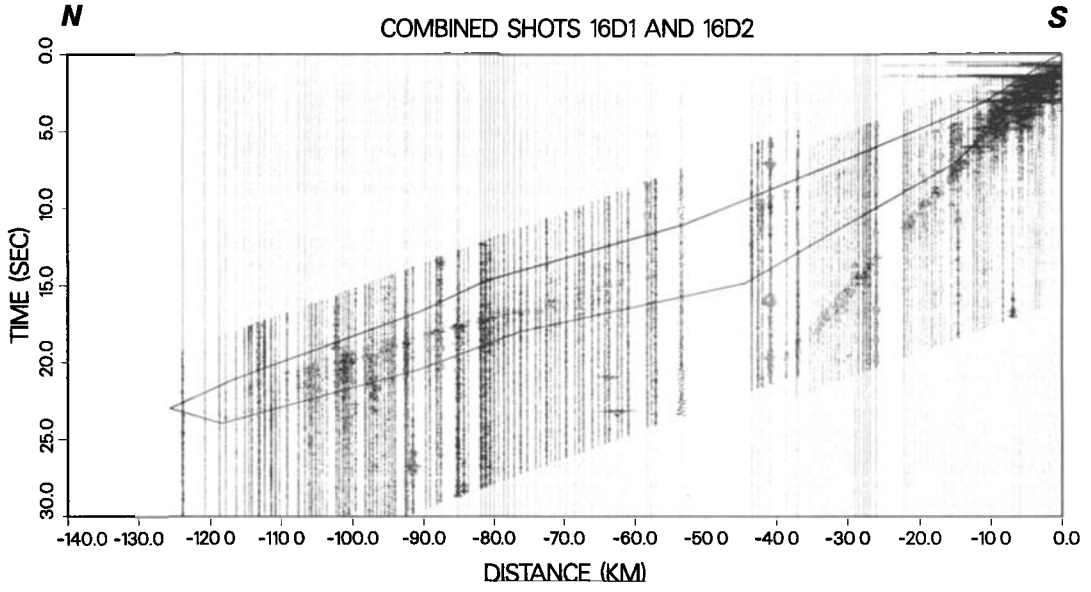

Fig. 2. Time versus offset seismic section for shot point 16. Both deployments one and two north of the shot point are plotted to show the continuous coverage from the northern end of the profile to the shot point 135 km to the south. Every other trace is plotted for clarity, and excessively noisy traces have not been plotted. Solid lines represent boundaries of the mutes applied in calculating Figure 4.

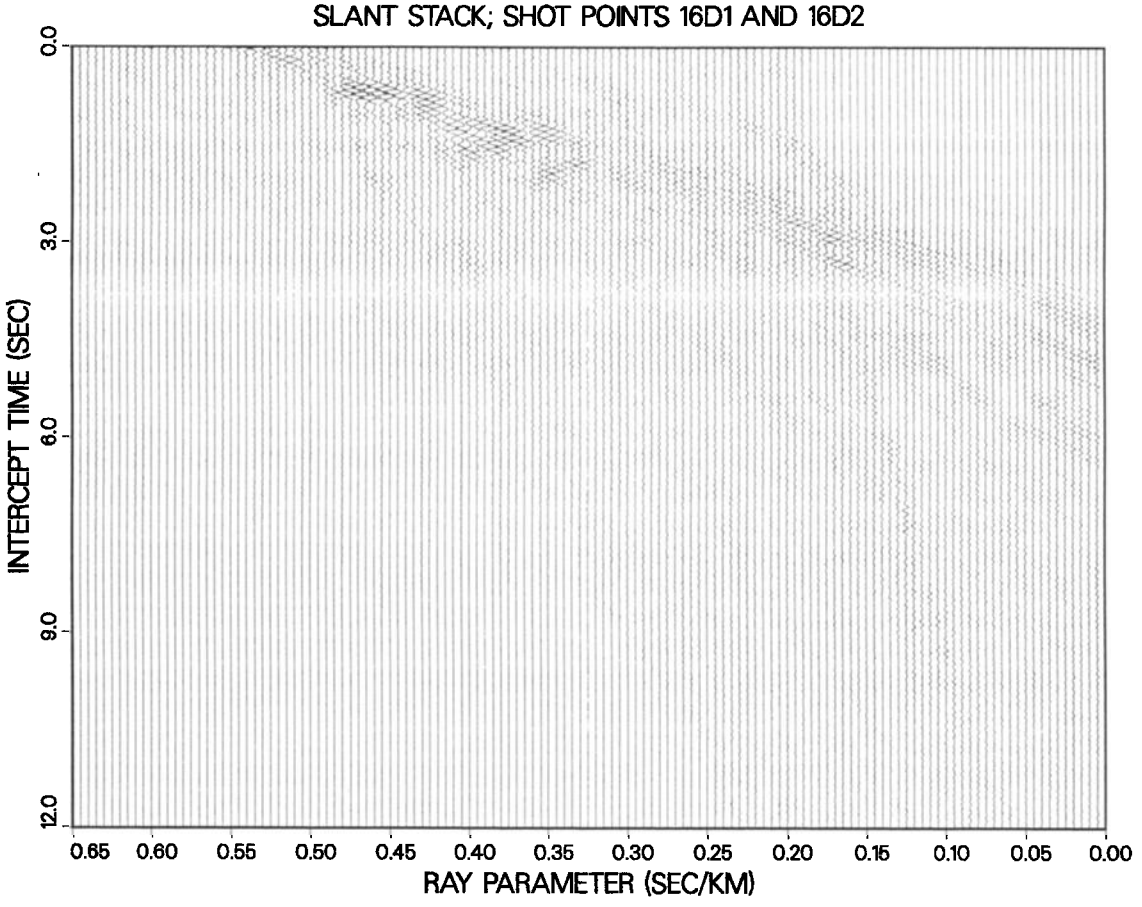

Fig. 3. Slant stack of data in Figure 2 using a standard slant stack algorithm in equal increments of ray parameter, with no enhancements.

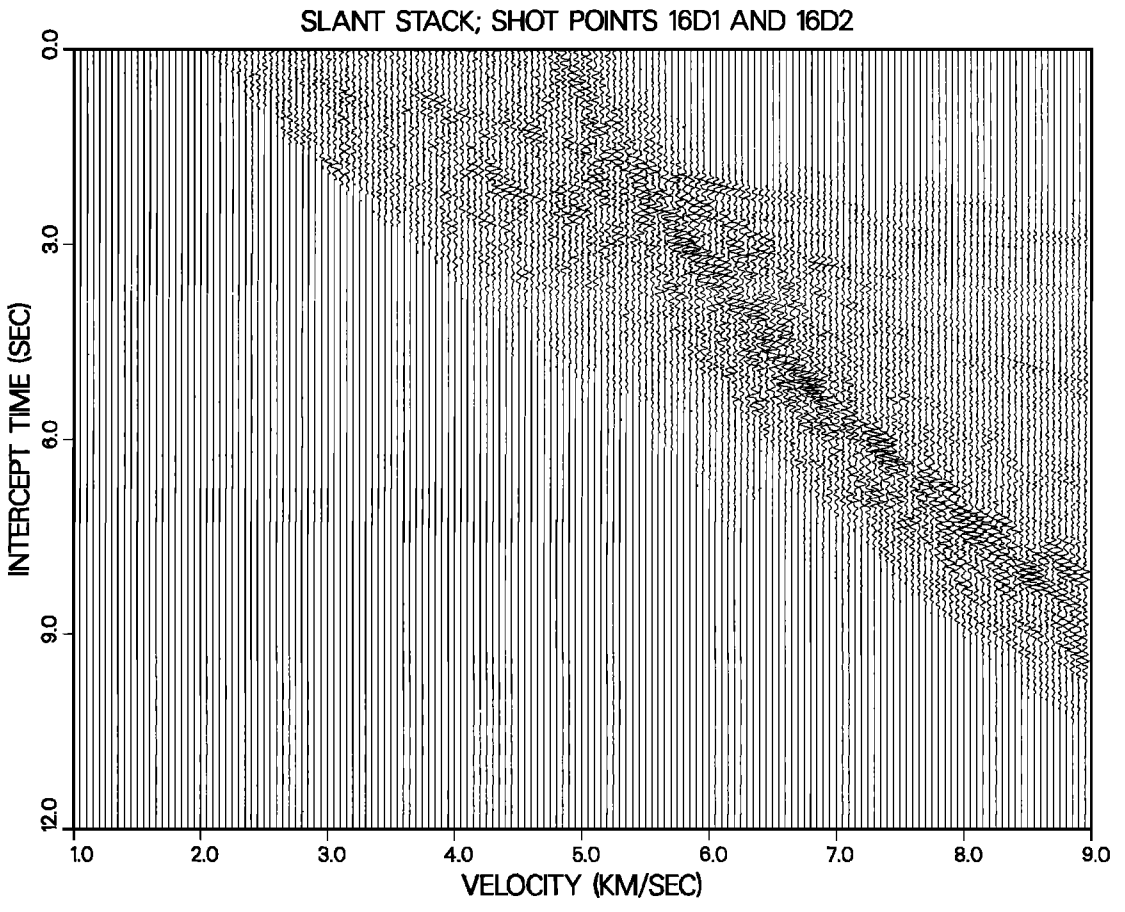

Fig. 4. Slant stack of data in Figure 2 with enhancements. The mutes outlined in Figure 2 were applied, the T-X seismograms were scaled by $X^{1.3}$ (X is offset distance) before stacking, and equal increments of velocity were used. Compare with Figure 3 to see the improvement in imaging the t curve.

6.0 s. This is followed at greater intercepts by other loci at about 7.3 km/s and 8.1 km/s and a weak locus at 8.4 km/s. Because of its velocity, the 8.1 km/s locus is likely to be the refracting velocity of the Moho. However, these locus points of energy have some sensitivity to the general signal to noise ratio of the data.

Maximum amplitude can be used to determine convergence in wave field data sets that have sufficiently high signal to noise ratio; however, the Ouachita data have a lower signal to noise ratio which forced a broadening of the definition of convergence. The definition of convergence used to obtain the final downward continued wave field in Figure 5 was modified so that the velocity function passed through one of the largest peaks on each trace and included as many maximum peaks as possible. An envelope around the velocity function that contains the maximum amplitudes serves as a useful estimate of the confidence interval of the true velocity function. The confidence intervals for this velocity envelope are approximately +/- 0.45 km/s. Given this velocity envelope, the slant stack model is consistent with the model presented by *Lutter and Nowack* [this issue]. Given the signal to noise ratio of the data, the velocity envelope is the most important constraint on the velocity models and tectonic interpretation provided by this analysis.

The power of slant stacking in constant velocity increments is apparent when comparing Figure 5 to the same downward continued wave field in equal ray parameter increments (see Figure 6). If the original slant stack was in equal ray parameter increments as in Figure 6, the aspects of the velocity structure apparent on Figure 5 would have been missed.

DISCUSSION AND INTERPRETATION

In order to make interpretations from the derived velocity model, a summary of the geotectonic history is first given. A more detailed description is given by *Lutter et al.* [this issue] and *Lutter and Nowack* [this issue]. Additionally, a geologic cross section showing the spatial relationships of tectonic elements discussed can be found in the interface inversion paper by *Lutter and Nowack* [this issue]. Cross-referencing this diagram should enhance the reader's understanding of the geotectonic history.

Eocambrian rifting is the first geologic event that is significant to the development of the southern continental margin [*Lillie et al.*, 1983; *Kruger and Keller*, 1986]. The rifting was associated with the initial opening of the proto-Atlantic Ocean and Gulf of Mexico. The late Cambrian through Devonian saw the development of an Atlantic-style passive margin which caught the majority of the sediments coming into the proto-Atlantic [*Houseknecht*, 1983]. Through this period, seafloor spreading continued and the ocean basin was sediment starved. This resulted in the slow deposition of a thick layer of pelagic sediments, including a large amount of cherts and other siliceous sediments [*Lowe*, 1975].

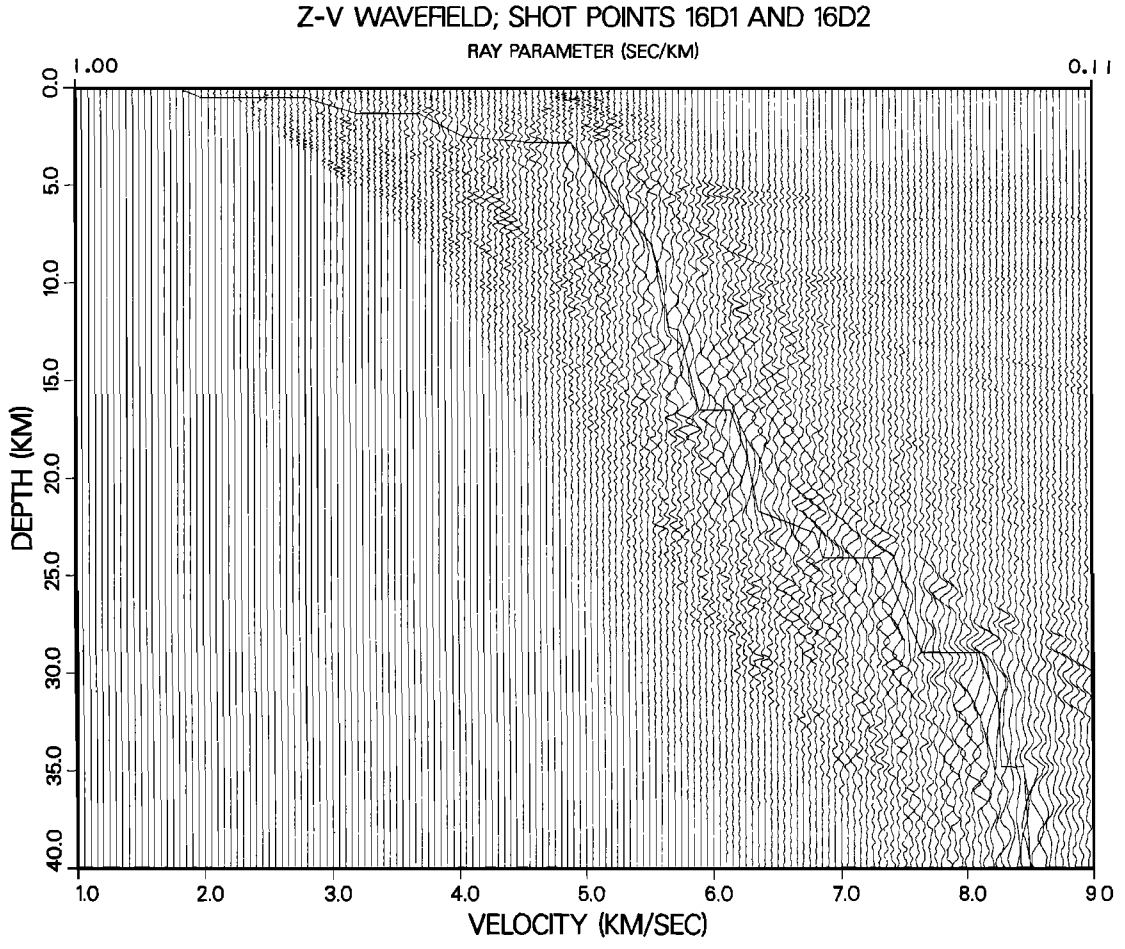

Fig. 5. Velocity-depth wave field obtained by downward continuation of τ-V wave field shown in Figure 4. The solid line that cuts across the wave field represents the final velocity-depth function for shot point gather 16.

In the Mississippian period, the expansion of the oceanic basin stopped and subduction began. The polarity of subduction is not agreed upon by all authors. The majority of authors support southward subduction [e.g., *Briggs and Roeder*, 1975; *Walper*, 1977; *Nelson et al.*, 1982; *Houseknecht*, 1983; *Lillie et al.*, 1983; *Plappert*, 1987; *Jardine*, 1988], but there have been other proposals for northward subduction [*Keller and Cebull*, 1973; *Morris*, 1971] as well as a subduction polarity reversal model [*Roeder*, 1973]. Although polarity of subduction is not clear, it is generally agreed that the slow sedimentation rates in the closing ocean basin ended in the Mississippian. This period was characterized by very rapid filling of the basin with flysch and volcanic debris associated with subduction [*Houseknecht*, 1983].

Subduction and contraction of the oceanic basin continued into the Pennsylvanian period, with even faster sedimentation rates than the Mississippian [*Walper*, 1977]. In the middle Pennsylvanian, North America collided with a southern landmass, which could have been an island arc complex, proto-South America or some exotic microcontinent [*Houseknecht*, 1983]. This collision resulted in the development of the Ouachita Mountains as well as the foreland Arkoma Basin [*Nelson et al.*, 1982]. The sediments from the uplifting Ouachita highlands were shed primarily into the Arkoma basin.

Deformation was complete by the conclusion of the Paleozoic, leaving a remnant basin on the south side of the Ouachita Mountains which was filled during the Permian with continental sediments. These sediments are not exposed anywhere at the surface but have been observed in deep drill hole data [*Woods and Addington*, 1973].

Rifting was again initialized in the Triassic, starting the opening of the present-day Gulf of Mexico and Atlantic Ocean. With the rifting, several grabens formed which cross the PASSCAL profile and were filled in with continental clastics and red beds of the Eagle Mills formation [*Vernon*, 1971].

The deposition of the gulf coastal plain sediments started in Jurassic and has generally prograded toward the south through the present [*Salvador and Buffler*, 1982]. The gulf coastal plain sediments are found at the surface over the entire data set.

The seven-layer final velocity model displayed in Figure 5 is interpreted within this geotectonic framework. The top layer of the model has a thickness of 0.5 km and the velocity varies from 1.8 to 2.0 km/s. This layer is interpreted to be the gulf coastal plain sediments of Tertiary age, which agrees with the surface geology and well data in the area [*Vernon*, 1971]. Layer 2 ranges from 0.5 to 1.2 km in depth, with velocities increasing from 2.8 km/s at the top to 3.2 km/s at the bottom. In accordance with other interpretations, such as *Jardine* [1988] and *Plappert* [1987], and well data in the area [*Vernon*, 1971], layer 2 corresponds to Jurassic and Cretaceous sediments of the gulf coastal plain. The third layer is the last of the Mesozoic sedimentary layers and is found in the one dimensional model from 1.3 to 2.8 km. Layer 3 is interpreted to be sediments of the Triassic Eagle Mills formation, which fills in grabens that

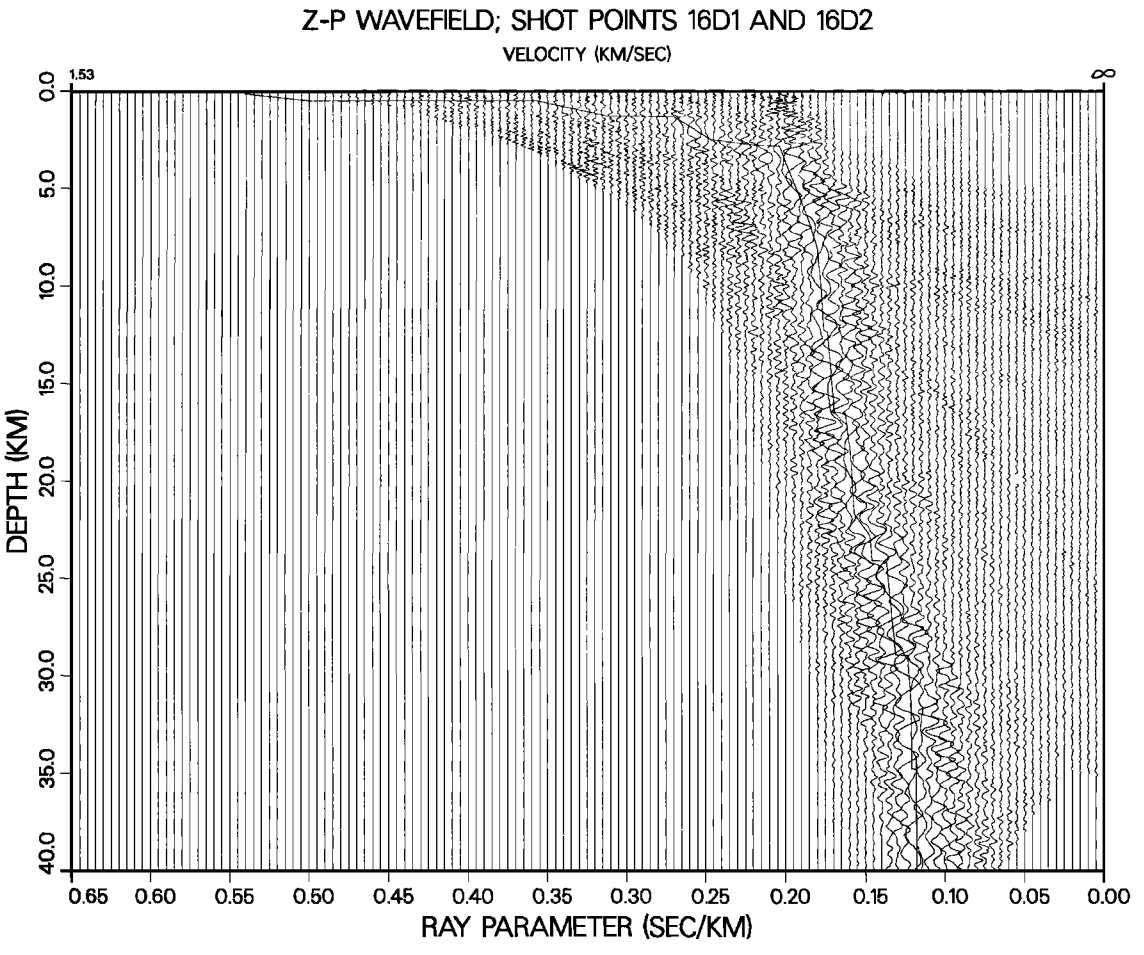

Fig. 6. Velocity-depth wave field obtained by downward continuation of slant stack wave field of shot point gather 16 stacked in equal increments of ray parameter. The velocity function used for downward continuation is the same as in Figure 5. Compare with Figure 5 to see how the imaging of most details is lost in Figure 6.

formed in association with the rifting open of the Gulf of Mexico [*Vernon*, 1971]. The boundaries and velocities given above for layer 3 most likely represent averages over the profile since the boundaries of a graben structure are likely to change laterally and vertically. The net thickness of the Mesozoic and Cenozoic cover in the slant stack model is approximately 0.75 km less than the forward ray trace model of *Jardine* [1988]. This is due to the averaging effect of the slant stack process over the lateral heterogeneities in the sedimentary section.

The fourth layer is a thick unit interpreted to be metamorphosed late Paleozoic sediments. The velocities in layer 4 start at 4.9 km/s at 28 km and increase nonlinearly to 5.9 km/s at 16.5 km. The changes in velocity within this layer may be due to changes in lithology but are probably at least partially related to increased depth of burial. Given this interpretation, these sediments may be dominated by the Mississippian and Pennsylvanian flysch deposits that were generated by the closing of the proto-Gulf of Mexico and the associated subduction and orogenic event which created the Ouachita mountains [*Keller et. al.*, 1989]. Additionally, at the top of layer 4, Permian sediments associated with the postcollision remnant basin may be likely. The upper third of layer 4 has a steeper velocity gradient than the rest of the unit and may be representative of these Permian sediments.

Layer 5 ranges in depth from 16.5 to 21.7 km, and the detailed velocity model ranges from 6.15 to 6.36 km/s. Other authors have seen a layer of similar velocity [*Lutter and Nowack*, this issue; *Chang and McMechan*, 1989]. Both interpret this layer as siliceous, deep-water pelagic sediments, or their metamorphic equivalents. This layer may be of lower Paleozoic age and deposited on the oceanic crust of the proto-Gulf of Mexico. The oceanic crust had from the Eocambrian through the Devonian to accumulate this very thick layer of pelagic sediments. Outcrops of a formation called the Arkansas Novacullite, a highly siliceous formation which has been interpreted to have been deposited in deep water, are found north of shot point 16 in the Ouachita mountains [*Lowe*, 1975]. Layer 5 may be equivalent to this formation.

The last crustal layer of the detailed velocity model varies in depth from 21.7 to 29.0 km. This layer, in accordance with its thickness and velocity, could be interpreted as the lower crustal layer of rifted-stage crust of a passive continental margin similar to the U.S. Atlantic margin [see *Klitgord et al.*, 1988; *Trehu et al.*, 1989]. *Plappert* [1987], *Jardine* [1988] and *Lutter and Nowack* [this issue] have a somewhat thicker lower crustal layer than is imaged by the slant stack method. Layer 6 of the detailed velocity model from the slant stack can be broken into two sublayers. From the top of the layer 6 to 24 km, the velocity varies from 6.8 to 6.87 km/s and from 24 km to the base at 29.0 km, the velocity varies from 7.3 to 7.6 km/s.

The final layer of the upper model is the mantle, starting at a depth of 29.0 km, with velocities ranging from 8.1 km/s at the

top and increasing to 8.5 km/s at 40.0 km. There is a slight suggestion of a step in the mantle velocities from 8.27 to 8.45 km/s at a depth of 35.0 km. This interpretation is based on the pattern of amplitude maximums, the locus of energy (representing a collapsed refraction) at approximately 8.4 to 8.5 km/s on Figure 4 and a weak arrival on shot point gather 16 at a slightly later arrival time than the Moho.

The slant stack velocity model can be compared with other velocity models for this section of the Ouachita data. These models include that of *Jardine* [1988], which was derived from matching travel time picks using forward ray tracing. *Lutter and Nowack* [this issue] based their model on an inversion of travel time picks for deep interface structure (see Figure 7). *Chang and McMechan* [1989] used a slant stack analysis, as this study did. However, *Chang and McMechan* [1989] considered only muted first arrivals in order to perform preliminary velocity analysis for use in further wavefield processing, and stacked in equal increments of ray parameter. The slant stack model presented here and the results of Chang and McMechan for shot point 16 agree closely to about 10 km depth, at which point there is some divergence. If both functions were plotted in reciprocal of velocity (ray parameter) versus depth, they would nearly overlap over the entire 40 km of the model. This reemphasizes the importance of stacking in equal velocity increments if a slant stack analysis is being used for velocity structure inversion. It is clear that the standard equal ray parameter sampling will miss the details of a faster velocity function.

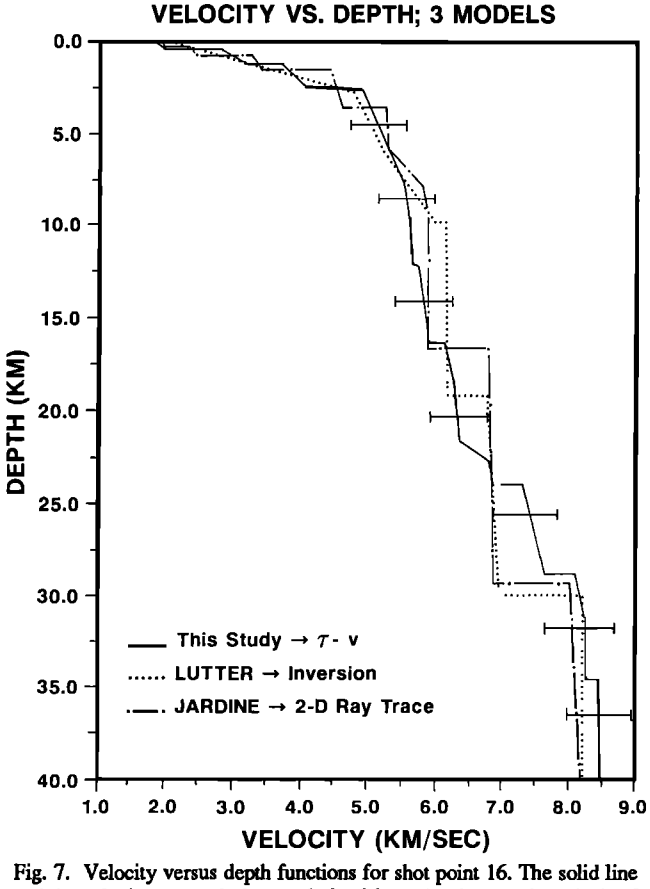

Fig. 7. Velocity versus depth functions for shot point 16. The solid line and the velocity uncertainties are derived from the slant stack analysis of this paper. The dotted line comes from *Lutter and Nowack* [this issue], the dot-dashed line comes from *Jardine* [1988].

Although there are differences between the alternative models and the detailed slant stacked model, the majority fall within the velocity envelope of the slant stack model, which suggests that the slant stack results are reasonable. However, the slant stack results do not eliminate the alternative interpretations on details of the velocity crustal structure. One of the differences of the detailed velocity model derived from the slant stack from previous models is the somewhat faster lower crustal velocities varying from 6.8-7.6 km/s. These faster lower velocities are consistent with a rift stage crust of a passive continental margin similar to the U.S. Atlantic margin [see *Klitgord et al.*, 1988; *Trehu et al.*, 1989].

Some of the differences between the slant stack model presented here and the other models can be attributed to estimating a two-dimensional model that is laterally heterogeneous with a one dimensional slant stack derived function as well as to the signal to noise ratio of the data. Additional disparities are introduced by the limitations associated with each of the different methods used to derive the various velocity functions. These limitations include, but are not limited to, hand-picking selected arrivals in the *Jardine* [1988], *Lutter et al.* [this issue] and *Lutter and Nowack* [this issue] models, the assumption of lateral homogeneity in the slant stack models, and the phase shift assumptions as well as aliasing and truncation effects of the slant stack algorithm. Given the assumptions of the different methods and the signal to noise ratio of the data, one of the most important results of the slant stack analysis is the consistency of the previous models with the slant stack velocity envelope.

CONCLUSION

The slant stack method can be a powerful tool in deriving a velocity versus depth function for a data set that does not have significant lateral heterogeneity. There are three primary steps that have been used to enhance a standard slant stack algorithm. First, for all data sets, proper muting is important since the τ curve used for downward continuation is composed only of postcritical reflections and refractions. Precritical reflections can serve a purpose in the downward continuation interpretation process because they will be flattened when the velocity structure is correct [*Clayton and McMechan*, 1981]. If the data are noisy however, muting the precritical reflections along with the noise in that region of the wavefield will have much greater utility.

The second step which can be taken for data sets with very long offsets is to scale the amplitudes by a factor equal to or greater than offset distance, which will increase the energy in the deeper parts of the velocity function. If the factor is equal to offset distance, it will compensate for geometrical spreading only, and if it is greater than offset distance, it can also compensate for attenuation. In this study, a factor of $X^{1.3}$ (where X is offset distance) was used to qualitatively balance average amplitudes across the shot point gather.

For higher velocities in the model, slant stacking in equal increments of velocity instead of ray parameter will image greater detail of a velocity function. When stacking in equal increments of ray parameter, many higher velocity details can not be imaged since for higher velocities, a small step in ray parameter is equivalent to a large increment in velocity. The change in velocity across some discontinuities will be smaller

than the sampling interval, making interpretation of these interfaces very difficult using equal increments of ray parameter.

The enhanced slant stack algorithm based on *Clayton and McMechan* [1981] was applied to shot point gather 16 of the PASSCAL Ouachita data set. The advantage of the slant stack method is that no picking of travel times is required as in other methods. Previous studies of the region have demonstrated that the structure beneath common shot point gather 16 is sufficiently laterally homogeneous to yield a meaningful velocity function using the slant stack method. However, as with other methods, there is sensitivity to signal to noise in the data. Previous velocity models are found to be consistent with the envelope of velocity functions imaged by the slant stack method. The locus of amplitudes within the τ curve are used to constrain a more detailed velocity model. This detailed velocity function, composed of seven layers, was found to be similar to other velocity models calculated for this area. The first three layers of the slant stack model are associated with sediments of the gulf coastal plain and range in age from Triassic to Tertiary in age. The next and thickest layer is associated with upper Paleozoic rocks and with the closing of the proto-Gulf of Mexico as subduction and orogenesis occurred. The fifth layer may have originated from siliceous pelagic sediments deposited in the sediment starved deep ocean of the proto-Gulf of Mexico. The determination of a more detailed velocity function from the slant stack velocity envelope suggests somewhat higher lower crustal velocities in the local crustal layer above the Moho. However, given the one-dimensional assumptions and signal to noise ratio of the data, the velocity envelope is the most important constraint on the velocity models and tectonic interpretation provided by the analysis.

Acknowledgments. Many of the ideas in this paper have evolved out of the work previously done on the Ouachita data by others, especially William Lutter, William Jardine, John Plappert and L.W. Braile, all of Purdue University. The paper was significantly improved by constructive reviews by T.M. Brocher and J.B. Diebold. This research has been supported by National Science Foundation grant EAR-8518147.

REFERENCES

Bessonova, E.N., V.M. Fishman, M.G. Shnirman, G.A. Sitnikova, and L.R. Johnson, The Tau method for inversion of travel times, *Geophys. J. R. Astron. Soc.*, 46, 87-108, 1976.

Bott, M.H.P., *The Interior of the Earth: Its Structure, Constitution, and Evolution*, Elsever Science, New York, 1982.

Bracewell, R.N., *The Fourier Transform and Its Applications*, 444 pp., McGraw-Hill, New York, 1978.

Braile, L.W., W.G. Jardine, G.R. Keller, S.H. Harder, and G.A. McMechan, Data report, 1986 PASSCAL Ouachita Lithospheric Seismology experiment, Inc. Res. Inst. for Seismol., Arlington, Va., 1987.

Briggs, G., and D. Roeder, Sedimentation and plate tectonics, Ouachita Mountains and Arkoma Basin, in *A Guidebook to the Sedimentology of Paleozoic Flysch and Associated Deposits, Ouachita Mountains - Arkoma Basin, Oklahoma*, pp.1-22, Dallas Geological Society, Dallas, Tex.,1975.

Brocher, T.M., W.C. Kempner, and J.F. Gettrust, A comparison of synthetic P-tau sections for proposed models of two ophiolites, *J. Geophys. Res.*, 87, 9355-9364, 1982.

Chang, Wen-Fong, and G.A. McMechan, Wave field processing of data from the 1986 Program for Array Seismic Studies of the Continental Lithosphere Ouachita experiment, *J. Geophys. Res.*, *94*, 17,781-17,792, 1989.

Chapman, C.H., Generalized radon transforms and slant stacks, *Geophys. J. R. Astron. Soc.*, *66*, 445-453, 1981.

Christensen, N.I., Compressional wave velocities in possible mantle rocks to pressures of 30 kilobars, *J. Geophys. Res.*, *79*, 407-412, 1974.

Clayton, R.W., and G.A. McMechan, Inversion of refraction data by wave field continuation, *Geophysics*, *46*, 860-868, 1981.

Diebold, J.B., and P.L. Stoffa, The travel time equation, tau-*P* mapping, and inversion of common midpoint data, *Geophysics*, *46*, 238-254, 1981.

Houseknecht, D.W., and J.A. Kacena, Tectonic and sedimentary evolution of the Arkoma Foreland Basin, in Tectonic-Sedimentary Evolution of the Arkoma Basin and Guidebook to Deltaic Facies, Hartshorne Sandstone, SEPM Midcontinent Section, 1, 3-33, 1983.

Jardine, W.G., Seismic reflection-refraction study over the southern margin of the Ouachita system of Arkansas and the adjacent gulf coastal plain, M.S. thesis, Purdue Univ., West Lafayette, Ind., 1988.

Keller, G.R., and S.E. Cebull, Plate tectonics and the Ouachita system in Texas, Oklahoma, and Arkansas, *Geol. Soc. Am. Bull.*, *83*, 1659-1666, 1973.

Keller, G.R., L.W. Braile, G.A. McMechan, W.A. Thomas, S.H. Harder, W.F. Chang, and W.G. Jardine, Crustal structure of the Ouachita orogenic belt determined by a PASSCAL wide-angle reflection/refraction experiment, *Geology*, *17*, 119-122, 1989.

Klitgord, K.D., D.R. Hutchinson, and H. Schouten, U.S. Atlantic Continental Margin: structural and tectonic framework, in *The Geology of North America, The Atlantic Continental Margin*, edited by R.E. Sheridan and J.A. Grow, vol. 1-2, Geological Society of America, Boulder, Colo., 1988.

Kruger, J.M., and G.R. Keller, Interpretation of crustal structure from regional gravity anomalies, Ouachita Mountains area and adjacent gulf coastal plain, *Am. Assoc. Pet. Geol. Bull.*, *70*, 667-689, 1986.

Lillie, R.J., K.D. Nelson, B. de Voogd, J.A. Brewer, J.E. Oliver, L.D. Brown, S. Kaufman, and G.W. Viele, Crustal structure of Ouachita Mountains, Arkansas: A model based on integration of COCORP reflection profiles and regional geophysical data, *Am. Assoc. Pet. Geol. Bull.*, *67*, 907-931, 1983.

Lowe, D.R., Regional controls on silica sedimentation in the Ouachita system, *Geol. Soc. Am. Bull.*, *86*, 1123-1127, 1975.

Lutter, W.J., and R.L. Nowack, Inversion for crustal structure using reflections from the PASSCAL Ouachita experiment, *J. Geophys. Res.*, this issue.

Lutter, W.J., R.L. Nowack, and L.W. Braile, Seismic imaging of upper crustal structure using travel times from the PASSCAL Ouachita experiment, *J. Geophys. Res.*, this issue.

McMechan, G. A., R.W. Clayton, and W.D. Mooney, Application of wave field continuation to the inversion of refraction data, *J. Geophys. Res.*, *87*, 927-935, 1982.

Morris, R.C., Sedimentary and tectonic history of the Ouachita Mountains, in Tectonics and Sedimentation, edited by W.R. Dickinson, *Spec. Publ. 22, Soc. Econ. Paleontol. Mineral.*, 120-142, 1971.

Nelson, K.D., R.J. Lillie, B. de Voogd, J.A. Brewer, J.E. Oliver, S. Kaufman, L. Brown, and G.W. Viele, COCORP seismic reflection profiling in the Ouachita Mountains of western Arkansas: Geometry and geologic interpretation, *Tectonics*, *1*, 413-430, 1982.

Phinney, R.A., and D.M. Jurdy, Seismic imaging of deep crust, *Geophysics*, *44*, 1637-1660, 1979.

Phinney, R.A., K.R. Chowdhury, and L.N. Frazer, Transformation and analysis of record sections, *J. Geophys. Res.*, *86*, 359-377, 1981.

Plappert, J.W., Processing and interpretation of near vertical and wide angle seismic reflection data from the PASSCAL Ouachita Lithospheric Seismic Study, M.S. thesis, Purdue Univ., West Lafayette, Ind., 1987.

Roeder, D.H., Subduction and orogeny, *J. Geophys. Res.*, *78*, 5005-5021, 1973.

Salvador, A., and R.T. Buffler, The Gulf of Mexico Basin, in *Perspectives in Regional Geological Synthesis*, edited by A.R. Palmer, pp. 157-162, Geological Society of America, Boulder, Colo., 1982.

Stoffa, P.L., P. Buhl, J.B. Diebold, and F. Wenzel, Direct mapping of seismic data to the domain of intercept time and ray parameter--A plane-wave decomposition, *Geophysics*, *46*, 255-267, 1981.

Trehu, A.M., A. Ballard, L.M. Dorman, J.F. Gettrust, K.D. Klitgord, and A. Schriener, Structure of the lower crust beneath the Carolina trough, U.S. Atlantic continental margin, *J. Geophys. Res.*, *94*, 10,585-10,600, 1989.

Vernon, R.C., Possible Future Petroleum Potential of Pre-Jurassic Western Gulf Basin, Future Petroleum Provinces of the United States--Their Geology and Potential, *Mem. Am. Assoc. Pet. Geol.*, *15*, 954-979, 1971.

Walper, J.L., Paleozoic Tectonics of the Southern Margin of North America, Trans. *Gulf Coast Assoc. Geol. Soc.*, *27*, 230-241, 1977.

Woods, R.D., and J.W. Addington, Pre-Jurassic geologic framework northern gulf basin, *Trans. Gulf Coast Assoc. Geol. Soc.*, *23*, 92-108, 1973.

J.A. Lyslo, Exxon Company, U.S.A., P.O. Box 120, Denver, CO 80201.

R.L. Nowack, Department of Earth and Atmospheric Sciences, Purdue University, West Lafayette, IN 47907.

(Received July 21, 1988;
revised December 15, 1989;
accepted December 18, 1989.)